

# Robust & Asymptotically Locally Optimal UAV-Trajectory Generation Based on Spline Subdivision

Ruiqi Ni<sup>1</sup>, Teseo Schneider<sup>2</sup>, Daniele Panozzo<sup>2</sup>, Zherong Pan<sup>3</sup>, Xifeng Gao<sup>1</sup>

**Abstract**—Generating locally optimal UAV-trajectories is challenging due to the non-convex constraints of collision avoidance and actuation limits. We present the first local, optimization-based UAV-trajectory generator that simultaneously guarantees validity and asymptotic optimality. **Validity:** Given a feasible initial guess, our algorithm guarantees the satisfaction of all constraints throughout the process of optimization. **Asymptotic Optimality:** We use a conservative piecewise approximation of the trajectory with automatically adjustable resolution of its discretization. The trajectory converges under refinement to the first-order stationary point of the exact non-convex programming problem. Our method has additional practical advantages including joint optimality in terms of trajectory and time-allocation, and robustness to challenging environments as demonstrated in our experiments.

## I. INTRODUCTION

Unmanned Aerial Vehicle (UAV) finds many real-world applications in inspection, rescue / search, and logistic automation. A key challenge in safe UAV-trajectory planning is to find locally optimal flying strategies, in terms of energy/time efficiency and smoothness, while accounting for various dynamic and kinematic constraints. A valid trajectory needs to satisfy two constraints: the trajectory needs to be physically realizable and the actuation limits must be respected (dynamic constraint), and the robot should maintain a safety distance from the boundary of the freespace (kinematic constraint). These two constraints combined define a non-convex and non-smooth feasible domain, which is notoriously difficult to handle for optimization-based motion planners [40], [25], [28]. For example, the safe-distance constraints are typically formulated using the distance function between a line-segment on the trajectory and an edge of the environmental obstacle, but this function is non-differentiable when the line-segment is nearly parallel with the edge, thus making it unsuitable for optimization techniques relying on first and second order derivatives.

Prior works tackle the non-convex, non-smooth constraints in one of three ways: infeasible recovery, relaxation, and global search. **Infeasible Recovery:** Nonlinear constrained optimizers, e.g. Sequential Quadratic Programming (SQP), have been used in [40], [35], [30] to directly handle non-convex constraints. These methods rely on the constraints' directional derivatives and penalty functions to pull infeasible solutions back to the feasible domain. However, their feasibility is not guaranteed: an example of a typical scenario of infeasible solutions involving an environment with multiple,

thin-shell obstacles is discussed in [28]. **Relaxation:** In [7], [5], relaxation schemes are used to limit the solutions to a (piecewise) convex and smooth subset. For example, the freespace is approximated by the union of convex subsets and a UAV-trajectory is represented by piecewise splines, where each piece is constrained in one convex subset. These relaxed formulations can be efficiently handled by modern (mixed-integer) convex optimization tools. However, these methods can only find sub-optimal solutions because the convex subset is a strict inner-approximation with a non-vanishing gap (and increasing the approximation power increases the algorithmic running time). For environments with narrow passages, relaxation can even turn a feasible problem into an infeasible one. **Global Search:** Kinodynamic-RRT\* [36] and its variants can find globally optimal UAV trajectories in a discrete space and stochastic gradient descend [15] will approach locally optimal solutions only if the descent direction is approximately by infinitely many samples. However, these algorithms take excessively large number of samples. To mitigate their computational cost, prior methods such as [21] have to terminate sampling early and then numerically rectify the solutions, and these numerical rectification methods still suffer from the limitations of infeasible recover or relaxation approaches.

**Main Results:** We propose a new formulation of local, optimization-based motion planning for UAV-trajectories with robustness and asymptotic optimality guarantee. Our method represents the UAV-trajectory using smooth curves, encoded as piecewise Bézier curves. For each Bézier piece, we formulate the collision-free constraints between its control polygon and the environmental geometry. We show that these constraints can be formulated as a summation of distance functions between geometric primitives (e.g. point-triangle and edge-edge pairs). Each distance function is differentiable when restricted to the feasible domain and the restriction can be achieved using a primal interior point method (P-IPM).

As compared with infeasible recovery methods that maintain both primal and dual variables, our primal-only formulation provides guaranteed solution feasibility throughout the entire process of optimization. This feature allows our planner to answer anytime re-planning queries as in [19] because the planner can be terminated at any iteration and return a feasible solution. And compared with relaxation-based methods, our method can asymptotically minimize the sub-optimality gap due to the control-polygon approximation of the true trajectory. This is achieved by using an adaptive Bézier subdivision scheme with user-controllable termination criterion.

Our method improves existing UAV planners in three

<sup>1</sup>Ruiqi Ni and Xifeng Gao are with Department of Computer Science, Florida State University (rn19g@my.fsu.edu and gao@cs.fsu.edu).

<sup>2</sup>Teseo Schneider and Daniele Panozzo are with the Department of Computer Science, New York University (teseo.schneider@nyu.edu and panozzo@nyu.edu).

<sup>3</sup>Zherong Pan is with the Department of Computer Science, University of Illinois Urbana-Champaign (zherong@illinois.edu).

ways: 1) Combined with RRT-style approaches, we can robustly rectify a feasible initial guess. 2) Starting from a feasible initial guess, our primal solver is guaranteed to preserve the homotopy class of the trajectory. This feature is useful, for example, for inspection planners where the order of inspection cannot be altered. 3) Our formulation achieves simultaneous optimality in trajectory shapes and time allocations. As compared with [30] where a separate decision variable is needed for time-allocation of each spline, we only need a global time re-scaling.

## II. RELATED WORK

Trajectory optimization for a general robotic system can be solved using dynamic programming [29], direct collocation [33], and path-integral control [15], [38]. While widely applicable, these methods require a search in a high-dimensional space and are thus computationally demanding and sensible to numerical failures. For the special case of UAV dynamics, a more robust and efficient approach has been proposed in [22], where the algorithm optimizes a reference position trajectory (global search) and then recovers the control inputs making use of differential flatness (local optimization). Our method follows the same strategy but offers the additional advantage of feasibility guarantees and locally optimality of the original non-convex optimization problem.

**Global Search** provides an initial trajectory that routes the UAV from a start to a goal position and usually optimizes the trajectory by minimizing a state- or time-dependent objective function. Global search can be accomplished using sampling-based motion planner [37], [18], mixed-integer programming [5], discrete search [20], and fast-marching method [10]. All these methods are approximating the globally optimal UAV-trajectory under some assumptions: optimal sampling-based motion planner approaches the optimal solution after a sufficient number of samples have been drawn; mixed-integer programming and discrete search restricts the decision space to a disjoint-convex or discrete subset, respectively; fast-marching methods discretize both the trajectory and the environment on a uniform grid. Global search is essential not only for providing an initial guess to the local optimization, but also for satisfying additional constraints. Typical constraints include visitation order [12], homotopy class [16], and coverage [13], [6]. These constraints can be formulated into the mixed-integer programming via additional binary decision variables [5] or into discrete search algorithms such as A\* by pruning trajectories that violate the constraints [20]. All these methods are orthogonal to our work and any global search method with the collision-free guarantee can be used as the initialization step of our method.

**Local Optimization** complements the global search by refining the trajectories in a neighborhood of the initial guess. This step lifts the restricted search space assumption in the global search and further minimizes the objective function in the continuous decision space, until a local optimal solution is attained. In addition, the local step ensures that the solution satisfies kinematics and dynamics constraints so that the trajectory is executable on hardware. All prior

works formulate the local step as a continuous or discrete optimization problem. The continuous problem can only be solved in the obstacle-free cases with a closed-form solution [36], [20]. In [10], [31], [35], obstacle-free constraints are relaxed to be convex and the resulting discrete optimization is guaranteed to be solvable using primal-dual interior point method (PD-IPM). In [39], [9], obstacle-free constraints are considered in its original, non-convex form, which is also solved using PD-IPM but without feasibility guarantee. In this work, we show that the feasibility guarantee can be provided using P-IPM.

**Time-Allocation** is an essential part of local optimization formulated as part of the dynamic constraints. Early works [27], [10] first optimize the shape of the trajectory and then allocate time for each discrete segment, and the resulting trajectory is sub-optimal with respect to the time variables. It has been shown that, for a fixed trajectory, optimal time-allocation can be achieved using bang-bang solutions computed via numerical integration [26]. The trajectories computed using numerical integration by [26] are locally optimal in either shape variables or time variables but not both at the same time. The latest works [30], [31] achieve shape-time joint optimality via bilevel optimization or weighted combination. We following [31] and optimize a weighted combination of shape and time cost functions.

## III. PROBLEM STATEMENT

We propose a new method for local optimization of UAV trajectories. A UAV moves along the center-of-mass trajectory  $p(t, w)$  with  $t \in [0, T]$  where  $T$  is the travel time and  $w$  is a set of decision variables. A local optimizer takes an initial trajectory as input and locally updates it to minimize a cost function:

$$\mathcal{O}(w, T) = \int_0^T c(p(t, w), t) dt + R(p(t, w), T), \quad (1)$$

where  $c(p, t)$  is the state-dependent cost (such as velocity, acceleration, jerk, or snap integrated along the trajectory) and  $R(p, T)$  is the terminal cost. In the meantime, a feasible UAV trajectory should satisfy a set of kinematic, dynamics, and application-dependent constraints. In this paper, we assume that dynamics constraints take the form of velocity and acceleration limits:

$$\|\dot{p}(t)\| \leq v_{max} \quad \|\ddot{p}(t)\| \leq a_{max} \quad \forall t \in [0, T], \quad (2)$$

which are semi-infinite constraints in the variable  $t$ . Here  $\{v, a\}_{max}$  are the maximum allowable velocity and acceleration. We further assume only the collision-free kinematic constraint that can take different forms depending on how obstacles are represented. Prominent environmental representations are point clouds and triangle meshes. These two representations can be uniformly denoted as a tuple of discrete elements  $\mathcal{E} = \langle \mathcal{P}, \mathcal{L}, \mathcal{T} \rangle$  where  $\mathcal{P}$  is a set of points,  $\mathcal{L}$  is a set of line segments, and  $\mathcal{T}$  is a set of triangles. The distance between a point  $x$  and the environment is denoted as  $d(x, \mathcal{E})$ . Our complete local trajectory optimization problem can be written as:

$$\underset{w, T}{\operatorname{argmin}} \mathcal{O}(w, T) \quad \text{s.t.} \quad \forall t \in [0, T] \begin{cases} \|\dot{p}(t)\| \leq v_{max} \\ \|\ddot{p}(t)\| \leq a_{max} \\ d(p(t), \mathcal{E}) \geq d_0 \end{cases}, \quad (3)$$

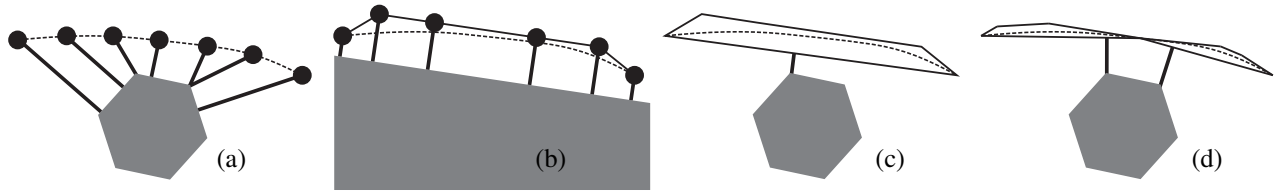


Fig. 1: A comparison of different treatments of collision constraints where the true obstacle is a hexagon. (a): The collision constraints are sampled on the UAV trajectory. (b): The obstacle is relaxed to a half-plane and distance constraints are imposed on the control points. (c): Our method imposes distance constraints between the convex hull of control points and the obstacle. (d): Our constraints can be refined by subdivision.

where  $d_0$  is an uncertainty-tolerating safety distance. Equation 3 is among the most challenging problem instances in operations research due to the semi-infinite constraints in time  $t$  and the non-smoothness of the function  $d$  [10], [14].

#### A. Trajectory Representation

We follow a common assumption that  $p(t, w)$  is a B-spline of degree  $M$ , which is a  $C^M$  curve. For convenience, we (locally) parametrize it as a collection Bézier curve. For a trajectory with  $N$  Bézier curve pieces each having order  $M$ , we need  $(M-2)N+3$  control points organized as in Figure 2, so  $w \in \mathbb{R}^{3((M-2)N+3)}$ . Unlike [30], [31], [35], this natural parameterization does not require additional linear constraints between adjacent curve pieces to ensure continuity.

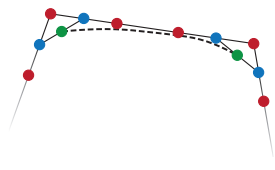


Fig. 2: Composite Bézier curve with  $M = 5$ ,  $w$  consists of red control points, blue points are linear interpolations of red points, and green points are linear interpolations of blue points. The UAV trajectory (dashed) is the Bézier curve with 2 red control points in the middle and one blue / green control point on each side.

#### B. Alternative Solutions

Prior work attempts to solve Equation 3 using various approximation schemes. These methods either significantly limit the solution space or fail to provide feasibility guarantee. As illustrated in Figure 1 (a), a first option [9] is to sample  $d(p(t), \mathcal{E})$  on UAV trajectories and then transform the sampled constraints into a soft penalty term, which is minimized using a first-order method. This approach does not guarantee a collision-free trajectory, even with a collision-free initial guess from global search. In Figure 1 (b), we illustrate the relaxation method [10] where the obstacle is relaxed to a half plane and distance constraints are imposed on the control points, which form a convex domain. If the half planes are chosen such that the convex domain satisfies the Slater's condition and Equation 1 is sufficiently smooth, optimizers such as [34] are guaranteed to return a locally optimal solution which is also a feasible solution of Equation 3 (due to the convex hull property of Bézier curves). However, the solution can be far from optimal in terms of Equation 3.

### IV. SUBDIVISION-BASED P-IPM

We propose an iterative algorithm, inspired by the recently proposed incremental potential contact handling scheme [17],

to find locally optimal solutions of Equation 3 with guaranteed feasibility.

#### A. Method Overview

The key idea of [17] is to use a primal-only (instead of primal-dual) interior point method to solve collision-constrained nonlinear optimization problems. This is achieved by transforming the collision-constraints into log-barrier functions, and reducing the problem to non-linear, unconstrained optimization. Although primal-dual approaches have better numerical stability in many problems, their convergence relies on sufficient smoothness and Mangasarian-Fromovitz constraint qualification (MFCQ) along the central path, which do not hold for collision constraints, often leading to failure in feasibility recovery. In contrast, given a feasible initial guess, line-search based, primal-only solvers are guaranteed (even in floating point implementations), to stay inside the feasible domain. The key to establish this invariance is the use of a robust line-search scheme that prevents solution from leaving the feasible domain, in our case rejecting iterations with a jump in homotopy class or violation of collision-free constraints. It has been shown in [17] that, for linearized trajectories, these safety checks can be performed using linear continuous collision detection (CCD). In this work, we extend this construction for motion planning with curved trajectories.

A safe line-search scheme ensures feasibility but does not guarantee local optimality, i.e. convergence to a first-order critical point. Assuming gradient-based optimizers are used, the additional requirement for local optimality is the objective function Equation 3 being differentiable, which is challenging due to the non-smoothness of the function  $d$ . Although SQP algorithms with gradient-sampling [4] can handle piecewise-smooth constraints such as  $d(p(t), \mathcal{E}) \geq d_0$ , they degrade the deterministic convergence guarantee to a probabilistic one in the sampling limit. In [17], [14], the authors note that two triangle meshes  $\mathcal{E}$  and  $\mathcal{E}'$  are  $d_0$ -apart if and only if any line segment pair in  $\mathcal{LL}' \triangleq \mathcal{L} \times \mathcal{L}'$  and point-triangle pair in  $\mathcal{PT}' \triangleq \mathcal{P} \times \mathcal{T}'$  or  $\mathcal{P}'\mathcal{T} \triangleq \mathcal{P}' \times \mathcal{T}$  are  $d_0$ -apart. As a result, the log-barrier of  $d$  is equivalent to the sum of log-barrier of distance functions between primitive pairs, which can be made differentiable after an arbitrarily small perturbation.

We plan to use primal-only algorithms to solve UAV trajectory's local optimization problems. To this end, the three preconditions of the primal-only method must hold. The first condition of a feasible initial guess holds trivially

by using an appropriate global searcher. With a fine-enough discretization granularity of signed distance field in [10], or that of sampled waypoints in [20], a feasible initial guess can be computed as long as a solution exists. For the second condition, although robust, exact continuous collision predicates exist for linear triangular meshes [3], [32], they have not been developed for polynomial curves. To bridge the gap, we propose to relax the exactness and resort to a conservative CCD scheme based on subdivision. For the third condition, i.e. the differentiability of the objective function, we propose to replace the trajectory with the union of convex hulls of the control polygons. These convex hulls are triangle meshes so the differentiable log-barrier between geometric primitives can be used. The accuracy of this approximation can be made arbitrarily high via adaptive subdivision.

### B. P-IPM Framework

We denote a Bézier curve as  $A(s)w$  with  $s \in [0, 1]$ . The convex hull of this curve has  $M + 1$  vertices,  $C_{M+1}^2$  edges, and  $C_{M+1}^3$  triangles at most. We denote  $\mathcal{P}(A)$  as the set of  $M + 1$  vertices,  $\mathcal{L}(A)$  as the set of  $C_{M+1}^2$  edges connecting all pair of vertices, and  $\mathcal{T}(A)$  as the set of  $C_{M+1}^3$  triangles connecting every 3 vertices, respectively, although some edges and triangles do not belong to the convex hull. A Bézier piece can be subdivided by a linear transformation of its control vertices into two pieces [8]: we denote the first piece as  $D_1A(s)w$  and the second piece as  $D_2A(s)w$ , where  $D_{1,2}$  are the fixed subdivision stencil constructed using the De-Casteljau's algorithm. Our adaptive subdivision scheme (Algorithm 2) will recursively apply these stencils until a stopping criterion is met. The result of the subdivision is another triangle mesh  $\mathcal{E}'$  which is the union of convex hulls of control points. As illustrated in Figure 1 (cd), given the environment  $\mathcal{E}$  (represented using either a point cloud or a triangle mesh) and  $\mathcal{E}'$ , we can define our log-barrier function as:

$$B(w, \mathcal{E}') \triangleq \sum_{\langle l, l' \rangle \in \mathcal{L}\mathcal{L}} \text{clog}(\text{dist}(l, l'(w)) - d_0) + \sum_{\langle p, t' \rangle \in \mathcal{P}\mathcal{T}'} \text{clog}(\text{dist}(p, t'(w)) - d_0) + \sum_{\langle p', t \rangle \in \mathcal{P}'\mathcal{T}} \text{clog}(\text{dist}(p'(w), t) - d_0), \quad (4)$$

where  $\text{dist}$  is the mollified, differentiable distance between a segment-segment or line-triangle pair, and  $\text{clog}$  is the clamped log-barrier function [17]:

$$\text{clog}(x) = \begin{cases} -(x - x_0)^2 \ln(\frac{x}{x_0}) & 0 < x \leq x_0 \\ 0 & \text{elsewhere,} \end{cases}$$

with  $x_0$  being the activation range. Although there are many terms in Equation 4, all the terms with  $\text{dist}(\bullet, \bullet)$  larger than  $d_0 + x_0$  must be zero. Therefore, we use a bounding volume hierarchy structure to efficiently prune all the zero terms.

We are now ready to summarize our main algorithm of P-IPM in Algorithm 3, which is a Newton-type method applied to the following unconstrained optimization problem:

$$\underset{w}{\text{argmin}} O(w, T) + \lambda B(w, \mathcal{E}'). \quad (5)$$

Here  $\lambda$  is the relaxation coefficient controlling the exactness

### Algorithm 1: Sub( $A(s)w, \mathcal{H}$ )

---

```

1: ▷ We denote the  $i$ th piece of  $p(t, w)$  as  $A_i(s)w$ 
2:  $\langle \mathcal{P}', \mathcal{L}', \mathcal{T}' \rangle \leftarrow \langle \emptyset, \emptyset, \emptyset \rangle$ 
3: if NeedSub( $A(s)w$ ) or  $A(s)w \in \mathcal{H}$  then
4:    $\mathcal{H} \leftarrow \mathcal{H} \cup \{A(s)w\}$ 
5:    $\langle \mathcal{P}', \mathcal{L}', \mathcal{T}' \rangle \leftarrow \langle \mathcal{P}', \mathcal{L}', \mathcal{T}' \rangle \cup \text{Sub}(D_1A(s)w, \mathcal{H})$ 
6:    $\langle \mathcal{P}', \mathcal{L}', \mathcal{T}' \rangle \leftarrow \langle \mathcal{P}', \mathcal{L}', \mathcal{T}' \rangle \cup \text{Sub}(D_2A(s)w, \mathcal{H})$ 
7: else
8:    $\langle \mathcal{P}', \mathcal{L}', \mathcal{T}' \rangle \leftarrow \langle \mathcal{P}(A), \mathcal{L}(A), \mathcal{T}(A) \rangle$ 
9: Return  $\langle \mathcal{P}(A), \mathcal{L}(A), \mathcal{T}(A) \rangle$ 

```

---

### Algorithm 2: TrajSub( $p(t, w), \mathcal{H}$ )

---

```

1: ▷ We denote the  $i$ th piece of  $p(t, w)$  as  $A_i(s)w$ 
2:  $\langle \mathcal{P}', \mathcal{L}', \mathcal{T}' \rangle \leftarrow \langle \emptyset, \emptyset, \emptyset \rangle$ 
3: for Iteration  $i = 1, \dots, N$  do
4:    $\langle \mathcal{P}', \mathcal{L}', \mathcal{T}' \rangle \leftarrow \langle \mathcal{P}', \mathcal{L}', \mathcal{T}' \rangle \cup \text{Sub}(A_i(s)w, \mathcal{H})$ 
5: Return  $\mathcal{E}' \leftarrow \langle \mathcal{P}', \mathcal{L}', \mathcal{T}' \rangle$ 

```

---

of constraint satisfaction. If the cost function is differentiable, the approximate Hessian has bounded eigenvalues, then P-IPM converges to a first-order critical point of Equation 5. Note that we keep a subdivision history  $\mathcal{H}$  to ensure that a curve subdivided in one P-IPM iteration will maintain the subdivision, which is essential for the convergence. Finally, the function SPD( $\bullet$ ) adjusts the Hessian matrix by clamping the negative eigenvalues to a small positive constant through a SVD to ensure positive-definiteness.

### Algorithm 3: P-IPM

---

**Input:**  $w_0, T_0$

```

1:  $\mathcal{H} \leftarrow \emptyset, w \leftarrow w_0, T \leftarrow T_0$ 
2: while  $\|\nabla_{w, T} O\|_\infty > \epsilon_g$  do
3:    $\mathcal{E}' \leftarrow \text{TrajSub}(p(t, w), \mathcal{H})$ 
4:   Calculate  $\nabla_{w, T} O, \nabla_{w, T}^2 O$ 
5:   Calculate  $d \leftarrow -\text{SPD}(\nabla_{w, T}^2 O)^{-1} \nabla_{w, T} O$ 
6:    $\langle w, T \rangle \leftarrow \text{Search}(\langle w, T \rangle, d)$ 
7: Return  $\langle w, T \rangle$ 

```

---

### C. Convergence Guarantee

The convergence guarantee of Algorithm 3 relies on the correct implementation of two functions: Search and NeedSub. The search function updates  $w$  to  $w'$  and ensures that the Wolfe's first condition holds and  $p(t, w)$  is homotopically equivalent to  $p(t, w')$ . Instead of using CCD which requires numerically stable cubic polynomial root finding, we use a more conservative check between the convex hull of geometric primitives before and after the update from  $w$  to  $w'$ . This procedure is outlined in Algorithm 4.

The NeedSubd function guarantees that the solution of Equation 5 asymptotically converge to that of Equation 3. When P-IPM is blocked by one of the log-barrier term in Equation 4, then the convex hull of some Bézier curve  $A(s)w$  is  $d_0 + x_0$  away from  $\mathcal{E}$ . This can imply either some point  $A(s)w$  ( $s \in [0, 1]$ ) is  $d_0 + x_0$  away from  $\mathcal{E}$  or the convex hull of the control polygon is a too coarse approximation of  $A(s)w$ . In the later case, we can bound the maximal distance between any  $A(s)w$  ( $s \in [0, 1]$ ) and its convex hull

of control polygon as  $d_0 + x_0 + \Delta(A, w)$ , where  $\Delta(A, w)$  is the diameter of the convex hull of the control polygon or any upper bound between a point  $A(s)w$  and its convex hull. A simple strategy that guarantees  $\epsilon$ -optimality is to always subdivide when 1)  $\Delta(A, w) > \epsilon$  and 2) the distance between the convex hull of  $A(s)w$  and  $\mathcal{E}$  is smaller than  $d_0 + x_0$ , where  $\epsilon$  is a user-provided optimality threshold. Note that condition 2) inherently induces an adaptive subdivision scheme where all the sub-trajectories that are sufficiently faraway from  $\mathcal{E}$  are not subdivided to save computation.

Algorithm 4: Search( $\langle w, T \rangle, d$ )

---

**Input:**  $\alpha, c_1 \in (0, 1)$

```

1: while True do
2:    $\langle w', T' \rangle \leftarrow \langle w, T \rangle + d$ 
3:   for  $\langle l, l' \rangle \in \mathcal{LL}'$  do
4:     if  $\text{ConvexHull}(l'(w), l'(w')) \cap l \neq \emptyset$  then
5:       Safe  $\leftarrow$  False
6:   for  $\langle p, t' \rangle \in \mathcal{PT}'$  do
7:     if  $\text{ConvexHull}(t'(w), t'(w')) \cap p \neq \emptyset$  then
8:       Safe  $\leftarrow$  False
9:   for  $\langle p', t \rangle \in \mathcal{P'T}$  do
10:    if  $\text{ConvexHull}(p'(w), p'(w')) \cap t \neq \emptyset$  then
11:      Safe  $\leftarrow$  False
12:   Safe  $\leftarrow$  True
13:   if Safe and  $O(w') < O(w) + c_1 < d, \nabla_w O >$  then
14:     Return  $w'$ 
15:   else
16:      $d \leftarrow \alpha d, \langle w', T' \rangle \leftarrow \langle w, T \rangle + d$ 
17: Return  $\langle w', T' \rangle$ 

```

---

#### D. Inexact P-IPM

A practical problem with Algorithm 3 is that we have to add all the  $C_2^M$  potential edges and  $C_3^M$  potential triangles of each convex hull of the control polygon to Equation 4. Even with a spatial hash acceleration, summing up so many terms is still time-consuming. To overcome this issue, we propose an inexact, yet preserving the guarantees of local optimality, version of P-IPM. Assuming the  $M + 1$  control points are ordered as:  $x_1, \dots, x_{M+1}$ , then the inexact P-IPM constructs Equation 4 using a single edge connecting  $x_1$  and  $x_{M+1}$  while removing all triangles, i.e.  $\mathcal{L}(A) = \{\langle x_1, x_{M+1} \rangle\}$  and  $\mathcal{T}(A) = \emptyset$ . Note that the edges and triangles are omitted in constructing Equation 4 but not in the Search function to ensure feasibility. This naive inexact P-IPM is not guaranteed to converge to the local minimum of Equation 5 because Algorithm 4 might not find a positive  $\alpha$  satisfying the first Wolfe's condition due to the conservative collision check. To ensure local optimality in the inexact case, we can simply increase  $d_0$  to  $d_0 + \epsilon$  then any geometric primitive not involved in Equation 4 is still  $d_0$  away from  $\mathcal{E}$  by triangular inequality and Algorithm 4 will not be blocked by collision checks.

#### E. Time-Optimality

Time efficacy can be formulated as a terminal cost such as  $R(p, T) = T$ , combining the semi-infinite velocity and acceleration bounds. Unlike [30], [10], that warp each Bézier piece of  $p(t, w)$  using a separate time parameter, we use a single, global time rescaling. In other words, the UAV flies

through each polynomial piece for  $T/N$  seconds. We argue that our parameterization has similar degrees of freedom as [30], [10]. This is because prior methods constraint each piece of the curve to a convex subset, so the arc-length of each piece is bounded away from zero. As a result, separate time parameters must be used to represent sharp velocity changes. However, we do not limit the arc-length of curve pieces, allowing sharp velocity changes by changing the arc-lengths. As illustrated in Figure 3, using different time allocations will result in similar trajectories.

We use the same principle as collision constraints to handle velocity and acceleration limits, by introducing a new set of log-barrier functions. For a subdivided curve piece  $A(s)w$ , its first and second  $s$ -derivatives are two new Bézier curves:  $\dot{A}(s)w$  and  $\ddot{A}(s)w$ , respectively. The convex hull of their control polygons and corresponding point, edge, triangle set are denoted as  $\langle \dot{P}, \dot{L}, \dot{T} \rangle$  for velocity and  $\langle \ddot{P}, \ddot{L}, \ddot{T} \rangle$  for acceleration. We can now define our log-barrier function approximating the velocity and acceleration limits as:

$$B_T(w, T) = \sum_{\dot{p} \in \dot{P}} \text{clog}(v_{max} - \|\dot{p}(w)\|_2 / (T/N)) + \sum_{\ddot{p} \in \ddot{P}} \text{clog}(a_{max} - \|\ddot{p}(w)\|_2 / (T^2/N^2)). \quad (6)$$

P-IPM now minimizes  $O(w, T) + \lambda B(w, \mathcal{E}) + \lambda B_T(w, T)$  to achieve joint optimality in terms of trajectory shape and time. Due to the convex hull property of Bézier curves, the finite value of  $B_T(w, T)$  implies that  $\|\dot{A}(s)w\|_2 \leq T v_{max}/N$  and  $\|\ddot{A}(s)w\|_2 \leq T^2 a_{max}/N^2$  for all  $s \in [0, 1]$  and subdivision can make the approximation arbitrarily exact. If desired, a separate subdivision rule can be used to control the exactness, e.g. always subdivide when  $\Delta(\dot{A}, w) > \epsilon$  or  $\Delta(\ddot{A}, w) > \ddot{\epsilon}$ . Finally, note that we need a feasible initial guess for  $T$  and a sufficiently large  $T$  is always feasible.

#### V. EXPERIMENTS

Our implementation uses C++11 and all results are computed using a single thread on a workstation with a 3.5 GHz Intel Core i9 processor. Our algorithm has the following parameters:  $\lambda$  of the collision avoidance barrier term,  $x_0$  of the activation range,  $d_0$  of the clearance distance,  $v_{max}$ ,  $a_{max}$ ,  $\epsilon$  of the subdivision threshold and  $\epsilon_g$  of the stopping criterion. We use  $\lambda = 10$ ,  $x_0 = 0.1$ ,  $d_0 = 0.1$ ,  $v_{max} = 2.0m/s$ ,  $a_{max} = 2.0m/s^2$ ,  $\epsilon = 0.1$ ,  $\epsilon_g = 1e-3$  for all experiments, unless otherwise specified in a particular test.

##### A. Comparisons

We compare our approach with the state-of-the-art gradient based method [9] and corridor based method [10]

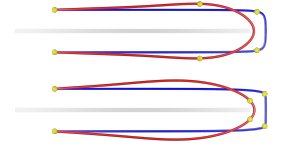


Fig. 3: We optimize a curve involving a sharp turn in the middle using two different time-allocations. Top: Each curve is assigned the same amount of time. Bottom: The middle curve is assigned less time. For both cases, our optimizer generates similar trajectories (yellow dots are the end points of Bézier curves).



on a set of scenes that are publicly downloadable from SketchFab [1]. We use the public implementations of both methods and did our best to tune our implementation to match the parameter settings of their methods, such as the orders of curves representing the trajectory, the energy term to measuring the smoothness of the trajectory (i.e. snap, jerk),  $v_{max}$ , and  $a_{max}$ . The implementation of [10] and [9] are run on dense point clouds sampled from the triangular meshes representing our scenes. Because of the complexity of the scenes listed in Table I, we did our best to manually tune waypoints to ensure that there will be a valid initial trajectory generated by the global search for all the methods, i.e. [10], [9], and ours.

Scene	Size	$L^{[10]}$	$T^{[10]}$	$C^{[10]}$	$L^{[9]}$	$T^{[9]}$	$C^{[9]}$	$L^*$	$T^*$	$C^*$
cave	1.4M/2.7M	70.5	144.3	420.4	82.6	73.3	0.5	56.0	30.3	927.9
site	0.4M/0	93.4	81.0	32.6	116.8	96.0	0.3	73.0	39.0	936.7
indoor1	0.2M/0.3M	-	-	-	14.8	18.0	0.2	13.5	9.1	140.1
indoor2	31K/58K	25.7	29.1	18.4	21.5	26.9	0.2	16.0	9.5	53.2
indoor3	17K/34K	25.1	24.1	27.4	22.8	23.6	0.1	19.7	11.3	76.4
indoor4	36K/68K	18.7	24.1	18.6	19.8	19.0	0.6	16.6	9.7	33.3
indoor5	81K/16K	23.2	38.5	21.9	25.2	26.3	0.2	21.5	12.4	153.9
indoor6	36K/68K	24.5	23.5	3.2	22.1	26.1	0.1	18.4	10.6	59.9

TABLE I: We profile the performance of [10], [9], and our method (denoted as  $*$ ) in terms of trajectory length  $L$ , arrival time  $T$ , and computational cost  $C$ . The size of each scene, in terms of its numbers of vertices and faces, is listed in the form of  $\#V/\#F$ . – denotes a failure in the provided program and the red color to highlight trajectories where the UAV collides with the scene.

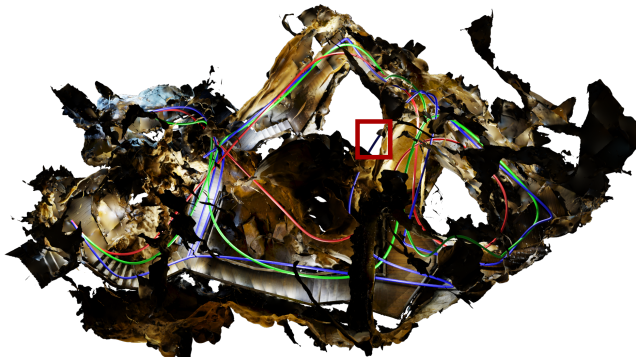


Fig. 4: In a complex cave environment, we compare UAV trajectories computed using our method (red), [9] (blue), and [10] (green) from the same initial guess. Both our method and [10] can generate feasible trajectories and our method finds a smaller objective function (e.g. smoother trajectory and smaller travel time as shown in Table I), while [9] converges to an infeasible solution (red box) that penetrates the environment.

As shown in Table I, our trajectories have the highest quality and far outperform the results of [10], [9]. Note that, since [9] doesn't have a collision-free guarantee even with a valid initial trajectory, their generated trajectories often penetrate the environments as highlighted in red in Table I. On the contrary, our method not only ensures a collision-free trajectory at every step during the optimization, but also guarantees that the trajectory is never closer to the obstacles than a user-specified safe distance. Although [10] requires only waypoints as input, we have to modify, in a trial-and-fail way, either the waypoints or the grid resolution used

by their approach so that their method can find a collision-free initialization to ensure that their trajectory optimization proceeds.

Note that [9], [10] achieve real-time computations and good quality trajectories for simple environments, however they struggle as the environments gets more complex. [9] tends to generate invalid trajectories with collisions between the UAV and the environment. [10] instead has a quickly growing runtime, since they have to reduce the failure rate of their initial trajectory generation by increasing the grid resolution, resulting in a similar efficiency as ours.

### B. Simulated UAV Flight in Challenging Environments

In the attached video, we simulate the UAV flying trajectory in the challenging environment of a scanned museum with a lot of narrow passages. The simulator is setup according to [23] and mimics the flying of a CrazyFlie nano-quadrotor. In the museum environment (represented using a dense triangle mesh with 1 million), we show that our optimization supports easily of the generated trajectory passing exactly user-specified waypoints. As demonstrated in the video, our optimization can generate a high quality trajectory that has tiny differences from the simulated path, allowing smooth UAV flying even during sharp turns.

## VI. CONCLUSION & LIMITATIONS

We propose a new approach of local UAV-trajectory optimization with guaranteed feasibility and asymptotic convergence to the semi-infinite problem. The key to our success is the primal-only optimizer equipped with an adaptive subdivision scheme for line search and constraint refinement. The line search scheme preserves the homotopy class and the constraint refinement guarantees sufficient closedness to the semi-infinite oracle (Equation 3). Using the same framework, we show that our method can be extended to achieve time-optimality. A limitation of our approach is that the trajectories might be slightly more conservative than necessary due to the conservativeness in our CCD check. This could be avoided with an exact curved CCD, which is an exciting avenue of future research. Besides, the bilevel formulation [30] provides more strict time optimality guarantee than our weighted objective function terms. It is possible to combine the two approaches by replacing our gradient with the their analytical gradient found from sensitivity analysis of the low-level problem. Finally, some prior works, e.g. [5], propose to tightly couple the global search with local optimization into a single algorithm solved with mixed-integer convex programming. Following similar reasoning, a mixed-integer nonlinear programming problem can be built on top of our method to achieve solutions with better optimality across multiple homotopy classes.

## REFERENCES

- [1] *SketchFab*, 2020 (accessed October 25, 2020). [Online]. Available: <https://sketchfab.com/>
- [2] T. G. Berry and R. R. Patterson, "The uniqueness of bézier control points," *Computer Aided Geometric Design*, vol. 14, no. 9, pp. 877–879, 1997.
- [3] T. Brochu, E. Edwards, and R. Bridson, "Efficient geometrically exact continuous collision detection," *ACM Trans. Graph.*, vol. 31, no. 4, July 2012. [Online]. Available: <https://doi.org/10.1145/2185520.2185592>

- [4] F. E. Curtis and M. L. Overton, "A sequential quadratic programming algorithm for nonconvex, nonsmooth constrained optimization," *SIAM Journal on Optimization*, vol. 22, no. 2, pp. 474–500, 2012.
- [5] R. Deits and R. Tedrake, "Efficient mixed-integer planning for uavs in cluttered environments," in *2015 IEEE international conference on robotics and automation (ICRA)*. IEEE, 2015, pp. 42–49.
- [6] C. Di Franco and G. Buttazzo, "Energy-aware coverage path planning of uavs," in *2015 IEEE international conference on autonomous robot systems and competitions*. IEEE, 2015, pp. 111–117.
- [7] W. Ding, W. Gao, K. Wang, and S. Shen, "Trajectory replanning for quadrotors using kinodynamic search and elastic optimization," in *2018 IEEE International Conference on Robotics and Automation (ICRA)*. IEEE, 2018, pp. 7595–7602.
- [8] G. E. Farin and D. Hansford, *The Essentials of CAGD*, 1st ed. USA: A. K. Peters, Ltd., 2000.
- [9] F. Gao, Y. Lin, and S. Shen, "Gradient-based online safe trajectory generation for quadrotor flight in complex environments," in *2017 IEEE/RSJ International Conference on Intelligent Robots and Systems (IROS)*, 2017, pp. 3681–3688.
- [10] F. Gao, W. Wu, Y. Lin, and S. Shen, "Online safe trajectory generation for quadrotors using fast marching method and bernstein basis polynomial," in *2018 IEEE International Conference on Robotics and Automation (ICRA)*, 2018, pp. 344–351.
- [11] J. Gravesen, "Adaptive subdivision and the length and energy of bézier curves," *Computational Geometry*, vol. 8, no. 1, pp. 13–31, 1997.
- [12] D. Grunzel and D. Jeffcoat, "Formulation and solution of the target visitation problem," in *AIAA 1st Intelligent Systems Technical Conference*, 2004, p. 6212.
- [13] J. A. Guerrero and Y. Bestaoui, "Uav path planning for structure inspection in windy environments," *Journal of Intelligent & Robotic Systems*, vol. 69, no. 1–4, pp. 297–311, 2013.
- [14] K. Hauser, "Semi-infinite programming for trajectory optimization with non-convex obstacles," in *International Workshop on the Algorithmic Foundations of Robotics*. Springer, 2018, pp. 565–580.
- [15] M. Kalakrishnan, S. Chitta, E. Theodorou, P. Pastor, and S. Schaal, "Stomp: Stochastic trajectory optimization for motion planning," in *2011 IEEE international conference on robotics and automation*. IEEE, 2011, pp. 4569–4574.
- [16] S. Kim, K. Sreenath, S. Bhattacharya, and V. Kumar, "Optimal trajectory generation under homology class constraints," in *2012 IEEE 51st IEEE Conference on Decision and Control (CDC)*, 2012, pp. 3157–3164.
- [17] M. Li, Z. Ferguson, T. Schneider, T. Langlois, D. Zorin, D. Panozzo, C. Jiang, and D. M. Kaufman, "Incremental potential contact: Intersection-and inversion-free, large-deformation dynamics," *ACM Trans. Graph.*, vol. 39, no. 4, July 2020. [Online]. Available: <https://doi.org/10.1145/3386569.3392425>
- [18] Y. Li, Z. Littlefield, and K. E. Bekris, "Asymptotically optimal sampling-based kinodynamic planning," *The International Journal of Robotics Research*, vol. 35, no. 5, pp. 528–564, 2016.
- [19] M. Likhachev, D. I. Ferguson, G. J. Gordon, A. Stentz, and S. Thrun, "Anytime dynamic a\*: An anytime, replanning algorithm," 2005.
- [20] S. Liu, N. Atanasov, K. Mohta, and V. Kumar, "Search-based motion planning for quadrotors using linear quadratic minimum time control," in *2017 IEEE/RSJ international conference on intelligent robots and systems (IROS)*. IEEE, 2017, pp. 2872–2879.
- [21] O. Mechali, L. Xu, M. Wei, I. Benkhaddra, F. Guo, and A. Senouci, "A rectified rrt\* with efficient obstacles avoidance method for uav in 3d environment," in *2019 IEEE 9th Annual International Conference on CYBER Technology in Automation, Control, and Intelligent Systems (CYBER)*. IEEE, 2019, pp. 480–485.
- [22] D. Mellinger and V. Kumar, "Minimum snap trajectory generation and control for quadrotors," in *2011 IEEE International Conference on Robotics and Automation*, 2011, pp. 2520–2525.
- [23] N. Michael, D. Mellinger, Q. Lindsey, and V. Kumar, "The grasp multiple micro-uav testbed," *IEEE Robotics Automation Magazine*, vol. 17, no. 3, pp. 56–65, 2010.
- [24] B. Mordukhovich and T. Nghia, "Constraint qualifications and optimality conditions for nonconvex semi-infinite and infinite programs," *Mathematical Programming*, vol. 139, no. 1–2, pp. 271–300, 2013.
- [25] C. Park, J. Pan, and D. Manocha, "Itomp: Incremental trajectory optimization for real-time replanning in dynamic environments," in *Twenty-Second International Conference on Automated Planning and Scheduling*, 2012.
- [26] Q.-C. Pham, "A general, fast, and robust implementation of the time-optimal path parameterization algorithm," *IEEE Transactions on Robotics*, vol. 30, no. 6, pp. 1533–1540, 2014.
- [27] C. Richter, A. Bry, and N. Roy, "Polynomial trajectory planning for aggressive quadrotor flight in dense indoor environments," in *Robotics Research*. Springer, 2016, pp. 649–666.
- [28] J. Schulman, Y. Duan, J. Ho, A. Lee, I. Awwal, H. Bradlow, J. Pan, S. Patil, K. Goldberg, and P. Abbeel, "Motion planning with sequential convex optimization and convex collision checking," *The International Journal of Robotics Research*, vol. 33, no. 9, pp. 1251–1270, 2014.
- [29] N. Slegers, J. Kyle, and M. Costello, "Nonlinear model predictive control technique for unmanned air vehicles," *Journal of guidance, control, and dynamics*, vol. 29, no. 5, pp. 1179–1188, 2006.
- [30] W. Sun, G. Tang, and K. Hauser, "Fast uav trajectory optimization using bilevel optimization with analytical gradients," in *2020 American Control Conference (ACC)*. IEEE, 2020, pp. 82–87.
- [31] G. Tang, W. Sun, and K. Hauser, "Enhancing bilevel optimization for uav time-optimal trajectory using a duality gap approach," in *2020 IEEE International Conference on Robotics and Automation (ICRA)*, 2020, pp. 2515–2521.
- [32] M. Tang, R. Tong, Z. Wang, and D. Manocha, "Fast and exact continuous collision detection with bernstein sign classification," *ACM Transactions on Graphics (TOG)*, vol. 33, no. 6, pp. 1–8, 2014.
- [33] O. Von Stryk, "Numerical solution of optimal control problems by direct collocation," in *Optimal control*. Springer, 1993, pp. 129–143.
- [34] Y. Wang, W. Yin, and J. Zeng, "Global convergence of admm in nonconvex nonsmooth optimization," *Journal of Scientific Computing*, vol. 78, no. 1, pp. 29–63, 2019.
- [35] Z. Wang, X. Zhou, C. Xu, J. Chu, and F. Gao, "Alternating minimization based trajectory generation for quadrotor aggressive flight," *IEEE Robotics and Automation Letters*, vol. 5, no. 3, pp. 4836–4843, 2020.
- [36] D. J. Webb and J. van den Berg, "Kinodynamic rrt\*: Optimal motion planning for systems with linear differential constraints," *arXiv*, pp. arXiv:1205.2012, 2012.
- [37] D. J. Webb and J. Van Den Berg, "Kinodynamic rrt\*: Asymptotically optimal motion planning for robots with linear dynamics," in *2013 IEEE International Conference on Robotics and Automation*. IEEE, 2013, pp. 5054–5061.
- [38] G. Williams, P. Drews, B. Goldfain, J. M. Rehg, and E. A. Theodorou, "Aggressive driving with model predictive path integral control," in *2016 IEEE International Conference on Robotics and Automation (ICRA)*. IEEE, 2016, pp. 1433–1440.
- [39] B. Zhou, F. Gao, L. Wang, C. Liu, and S. Shen, "Robust and efficient quadrotor trajectory generation for fast autonomous flight," *IEEE Robotics and Automation Letters*, vol. 4, no. 4, pp. 3529–3536, 2019.
- [40] M. Zucker, N. Ratliff, A. D. Dragan, M. Pivtoraiko, M. Klingensmith, C. M. Dellin, J. A. Bagnell, and S. S. Srinivasa, "Chomp: Covariant hamiltonian optimization for motion planning," *The International Journal of Robotics Research*, vol. 32, no. 9–10, pp. 1164–1193, 2013.

## CONVERGENCE ANALYSIS

We analyze the convergence behavior of Equation 3 without velocity / acceleration limits, the case with velocity / acceleration limits is similar. Note that there are three parameters of P-IPM:  $\gamma$ ,  $x_0$ , and  $\epsilon$ .

### A. Perturbed Optimality

We rewrite Equation 3 as a smooth SIP by augmenting the index set:

$$\underset{w}{\operatorname{argmin}} O(w) \quad \text{s.t.} \quad \forall t \in [0, T], q \in \mathcal{E} \quad d(p(t), q) \geq d_0, \quad (7)$$

which is equivalent to Equation 3 (without velocity / acceleration limits). We abbreviate  $O(w, T)$  as  $O(w)$  from now. According to [24], the exact KKT condition at  $w$  requires an index set  $I(w) = \{ \langle t, q \rangle \mid d(p(t, w), q) = d_0 \}$  on which:

$$0 = \nabla_w O(w) + \sum_{\langle t, q \rangle \in I} \lambda_{\langle t, q \rangle} \nabla_w d(p(t, w), q) \quad (8)$$

$$\text{s.t.} \quad \lambda_{\langle t, q \rangle} \leq 0.$$

A perturbed KKT condition, denoted as  $\text{KKT}(\epsilon_1, \epsilon_2)$ , could be defined on an inexact index set  $\tilde{I}(w) = \{ \langle t, q \rangle \mid d_0 - \epsilon_1 \leq d(p(t, w), q) \leq d_0 + \epsilon_1 \}$  on which:

$$0 = \nabla_w O(w) + \sum_{\langle t, q \rangle \in \tilde{I}} \lambda_{\langle t, q \rangle} \nabla_w g_{\langle t, q \rangle}(w)$$

$$\text{s.t.} \quad \lambda_{\langle t, q \rangle} \leq 0$$

$$\| \nabla_w g_{\langle t, q \rangle}(w) - \nabla_w d(p(t, w), q) \| \leq \epsilon_2.$$

### B. Solution Sequence

With each set of parameters, and from initial guess  $w_0$ , Algorithm 3 will return a solution denoted as  $w(\gamma, x_0, \epsilon, w_0)$ . By introducing another parameter  $\beta \in (0, 1)$ , we can construct a sequence  $\{w_k \mid k = 1, 2, \dots\}$  such that  $w_k \triangleq w(\beta^k \gamma, \beta^k x_0, \beta^k \epsilon, w_{k-1})$ . If we can solve P-IPM to local minimum, then the following function diminishes at  $w_k$ :

$$0 = \nabla_w O(w_k) + \sum_{i \in S_k} \lambda_i^k \nabla g_i(w_k) \quad (9)$$

$$\lambda_i^k = \beta^k \lambda \nabla \log(g_i(w_k)) \leq 0,$$

where  $g_i(w)$  are functions of form  $\text{dist}(\bullet, \bullet) - d_0$ , and  $S_k$  is the set of indices of non-zero log-barrier terms. From the definition of  $\log$ , it is obvious that  $0 \leq g_i(w_k) \leq \beta^k x_0$  for all  $i \in S_k$ .

We will take the following assumption:

**Assumption 6.1:**  $\{w_k \mid k = 1, 2, \dots\}$  and  $\{p(t, w_k) \mid t \in [0, T], k = 1, 2, \dots\}$  are bounded.

The following lemma is obvious under Assumption 6.1, which essentially shows that  $w_k$  progressively approach KKT with diminishing error:

**Lemma 6.2:** Assuming Assumption 6.1,  $w_k$  satisfies  $\text{KKT}(L_1\beta^k\epsilon + \beta^k x_0, L_2\beta^k\epsilon)$ .

*Proof:* Under the bounded assumption  $d(x, y)$  is a Lipschitz-continuous function in  $x$  with constant  $L_1$  and  $\nabla_x d(x, y)$  is another Lipschitz-continuous function in  $x$  with constant  $L_2$ . We consider the special form of  $g_i(w_k) = \text{dist}(\bullet, \bullet) - d_0$ . Although  $\bullet$  can be a point, a line segment, or a triangle, there must be a point on the sub-trajectory's convex hull  $p_i^k$  and a point  $q_i^k \in \mathcal{E}$  that realize  $g_i$ , i.e.  $g_i(w_k) = d(p_i^k, q_i^k) - d_0$  and  $\nabla g_i(w_k) = \nabla_w d(p_i^k, q_i^k)$ . Further, due to our subdivision condition, there must be a point on the exact trajectory  $p(t_i^k, w_k)$  such that  $\|p_i^k - p(t_i^k, w_k)\| < \beta^k\epsilon$ . In other words, each  $g_i(w_k)$  is associated with three variables: a point on sub-trajectory's convex hull  $p_i^k$ , a point on the exact trajectory  $p(t_i^k, w_k)$ , and a point on the environment  $q_i^k$ . We have the following results:

$$\begin{aligned} & -L_1\beta^k\epsilon + d_0 \\ & \leq -\|d(p(t_i^k, w_k), q_i^k) - d(p_i^k, q_i^k)\| + d(p_i^k, q_i^k) \\ & \leq d(p(t_i^k, w_k), q_i^k) \\ & \leq \|d(p(t_i^k, w_k), q_i^k) - d(p_i^k, q_i^k)\| + d(p_i^k, q_i^k) \\ & \leq L_1\beta^k\epsilon + \beta^k x_0 + d_0 \\ & \quad \|\nabla g_i(w_k) - \nabla_w d(p(t_i^k, w_k), q_i^k)\| \\ & = \|\nabla_w d(p_i^k, q_i^k) - \nabla_w d(p(t_i^k, w_k), q_i^k)\| \leq L_2\beta^k\epsilon, \end{aligned}$$

so  $w_k$  satisfies  $\text{KKT}(L_1\beta^k\epsilon + \beta^k x_0, L_2\beta^k\epsilon)$  by choosing  $\tilde{I}(w_k) = \{< t_i^k, q_i^k >\}$ ,  $g_{< t_i^k, q_i^k >} = g_i$ , and  $\lambda_{< t_i^k, q_i^k >} = \lambda_i^k$ . ■

Next, we consider a convergent subsequence  $\{w_{k(j)} | j = 1, 2, \dots\} \rightarrow w_*$  (there must be at least one due to Assumption 6.1). Although the exactness of KKT satisfaction at  $w_{k(j)}$  can be made arbitrarily close to zero, we emphasize that  $w_*$  might not satisfy KKT condition of Equation 7, of which a counterexample can be easily constructed at some  $w_*$  without LICQ. To setup the KKT condition at  $w_*$ , we need an additional assumption of bounded Lagrangian multiplier:

**Assumption 6.3:** For a constant  $L_3$  independent of  $k$ , we have  $\|\nabla \text{clog}(g_i(w_k))\| \leq L_3$ .

### C. Subdivision Limit

In this section, we show that after subdivision, the number of log-barrier terms grows reciprocally with  $\beta^k$ . This result is due to the fact that the arc length of a Bézier curve is lower bounded by length of its control polygon according to [11], which will be used to prove the KKT satisfaction at  $w_*$ .

**Lemma 6.4:** Under Assumption 6.1, there exists a constant  $L_4$  independent of  $k$ , such that for any convergent subsequence  $\{w_{k(j)} | j = 1, 2, \dots\} \rightarrow w_*$ , the number of log-barrier terms involved in Equation 8 is upper bounded by  $L_4/\beta^{k(j)}$ , i.e.  $|S_{k(j)}| < L_4/\beta^{k(j)}$ .

*Proof:* To show this result, we need to adopt a similar technique as [11]. We use the same notations as those in the main paper, i.e. the UAV trajectory is represented by  $N$

Bézier curves each of order  $M$  with parameter  $s \in [0, 1]$ . For simplicity and without a loss of generality, we assume  $N = 1$ . We introduce the arc-length of a Bézier curves as:

$$\Sigma(w) = \int_0^1 \|\dot{A}(s)w\| ds.$$

Notice that  $\Sigma(w)$  is subdivision invariant. In other words, summing up  $\Sigma(w)$  for each sub-curve after subdivision yields the arc-length of the entire curve. By the convergence of  $w_{k(j)}$  and the continuity of  $\Sigma(w)$ , we can further choose sufficiently large  $j_\Sigma$  such that  $\Sigma(w_{k(j)}) < 2\Sigma(w_*)$  for all  $j > j_\Sigma$ .

Next, we need to bound the arc-length of each sub-curve. By Cauchy-Schwarz inequality, we have:

$$\begin{aligned} \Sigma(w) &= \int_0^1 \|\dot{A}(s)w\| ds \geq \sqrt{\int_0^1 \|\dot{A}(s)w\|^2 ds} \\ &= \sqrt{w^T \left[ \int_0^1 \dot{A}(s)^T \dot{A}(s) ds \right] w} \triangleq \sqrt{w^T H w} \\ &\triangleq \sqrt{w^T D^T \bar{H} D w} \geq \sigma_{\min}(\sqrt{\bar{H}}) \|Dw\|. \end{aligned}$$

Here  $D$  is the stencil that extracts the edges of control polygon, defined as:

$$D \triangleq \begin{pmatrix} I & -I & & \\ & I & -I & \\ & & \ddots & \ddots \\ & & & I & -I \end{pmatrix}.$$

We further emphasize that  $\sigma_{\min}(\sqrt{\bar{H}}) > 0$ , i.e.  $\bar{H}$  is strictly positive definite. This is because the derivative of a Bézier curve of order  $M$  is another Bézier curve of order  $M - 1$ , with control points being  $Dw$ . In addition, a Bézier curve is uniquely defined by its control polygons [2], so that if  $w^T D^T \bar{H} D w = 0$ , then  $Dw = 0$ , which further implies that  $\bar{H}$  has a full rank.

We then bound the term  $\|Dw\|$ , which can be done using our subdivision rule. We first notice that  $\|Dw\|$  is the total length of control polygon and we know that the total length of control polygon must be larger than the diameter of a control polygon  $\Delta(A, w)$ . (This is because the diameter of a polytope is realized on two vertices, the distance between which is smaller than the path connecting all vertices.) We consider a subdivision that is done on  $A(s)w$  to derive two sub-curves with control points:  $D_{1,2}w$ , respectively. If  $\|DD_1w\| \leq \beta^{k(j)}\epsilon / \max(\sigma_{\max}(D_1), \sigma_{\max}(D_2))$ , then

$$\begin{aligned} \Delta(A, w) &\leq \|Dw\| \\ &\leq \beta^{k(j)}\epsilon \frac{\sigma_{\max}(D_1)}{\max(\sigma_{\max}(D_1), \sigma_{\max}(D_2))} \leq \beta^{k(j)}\epsilon, \end{aligned}$$

and a similar result holds for  $\|DD_2w\|$ . However, it is impossible for  $\Delta(A, w) \leq \beta^{k(j)}\epsilon$  because our subdivision rule will prevent further subdivision. As a result, we must have that every curve that is subdivided to the limit satisfies the following condition:

$$\|Dw\| \geq \frac{\beta^{k(j)}\epsilon}{\max(\sigma_{\max}(D_1), \sigma_{\max}(D_2))}.$$

Combining this result with the lower bound of arc-length,



we have:

$$\Sigma(w) \geq \frac{\beta^{k(j)} \epsilon \sigma_{\min}(\bar{H})}{\max(\sigma_{\max}(D_1), \sigma_{\max}(D_2))}.$$

Finally, we can prove by contradiction. If no constant  $L_4$  can be found, then we can define:

$$L_4 \triangleq \frac{2\Sigma(w_{k(j)}) \max(\sigma_{\max}(D_1), \sigma_{\max}(D_2))}{\epsilon \sigma_{\min}(\bar{H})},$$

and find infinitely many  $j$  such that  $|S_{k(j)}| \geq L_4/\beta^{k(j)}$ . For each of these  $w_{k(j)}$ , their arc length satisfies  $\Sigma(w_{k(j)}) \geq 2\Sigma(w_*)$ , which contradicts the convergence of  $\Sigma(w_{k(j)})$ . ■

#### D. KKT Condition at $w_*$

It is obvious that  $w_*$  is a feasible point of Equation 7. We now prove by contradiction that KKT condition (Equation 8) holds at  $w_*$ . Suppose otherwise that KKT condition does not hold at  $w_*$ , then there must be a unit direction  $v$  such that:

$$\begin{aligned} v^T \nabla_w O(w_*) &= \epsilon_3 < 0 \\ v^T \nabla_w d(p(t, w_*), q) &\geq 0 \quad \forall < t, q > \in I(w_*). \end{aligned} \quad (10)$$

We prove that  $v$  must be a descend direction at  $w_{k(j)}$  for sufficiently large  $j$ , contradicting the fact that  $w_{k(j)}$  is a local minimum of P-IPM. Note that for any point  $p(t_i^{k(j)}, w_{k(j)})$ , it is not possible for  $d(p(t_i^{k(j)}, w_{k(j)}), q_i^{k(j)}) = d_0$  as the log-barrier will be infinite otherwise, i.e. we cannot reach any point in the index set of  $w_*$ , but we can bound their distance using the following lemma:

**Lemma 6.5:** Under Assumption 6.1, given any  $\epsilon_4 > 0$ , there is a large enough  $j(\epsilon_4)$ , such that for all  $j \geq j(\epsilon_4)$  and  $\text{clog}(g_i(w_{k(j)})) > 0$ , we can find some  $< t, q > \in I(w_*)$  satisfying:

$$\|p(t_i^{k(j)}, w_{k(j)}) - p(t, w_*)\| \leq \epsilon_4.$$

*Proof:* We proof by contradiction. Suppose otherwise, there exists some  $\epsilon_4 > 0$  such that for any  $j_0$ , we can always find some  $j > j_0$  and  $\text{clog}(g_i(w_{k(j)})) > 0$  where  $\|p(t_i^{k(j)}, w_{k(j)}) - p(t, w_*)\| > \epsilon_4$  for all  $< t, q > \in I(w_*)$ . Then we can construct an infinite sub-sequence of form  $\{p(t_i^{k(j)}, w_{k(j)})\}$  in which every point is at least  $\epsilon_4$  away from the index set  $I(w_*)$ . Due to Assumption 6.1, there will be a convergent subsequence of  $\{p(t_i^{k(j)}, w_{k(j)})\}$ , the limit of which denoted as  $p(t_*, w_*)$ . We have  $d(p(t_*, w_*), \mathcal{E}) = 0$  so  $p(t_*, w_*)$  belongs to the index set. Further,  $p(t_*, w_*)$  is at least  $\epsilon_4$  away from the index set, a contradiction. ■

We can now present our main result, which involves bounding each term in Equation 9:

**Lemma 6.6:** Under Assumption 6.1 and Assumption 6.3, for any convergent subsequence  $\{w_{k(j)} | j = 1, 2, \dots\} \rightarrow w_*$ , a unit vector satisfying Equation 10 is a descend direction at  $w_{k(j)}$  for sufficiently large  $j$ .

*Proof:* We start from the constraint gradient  $\nabla g_i$ . Since we use a fixed number of Bézier curves, a point on the curve  $p(t, w)$  is a uniformly Lipschitz continuous function of  $w$  and we denote the  $t$ -independent constant as  $L_5$ . We divide the directional derivative of  $\nabla g_i$  along  $v$  into three terms, each

equipped with a diminishing bound:

$$\begin{aligned} & v^T \nabla g_i(w_{k(j)}) \\ &= v^T (\nabla g_i(w_{k(j)}) - \nabla_w d(p(t_i^{k(j)}, w_{k(j)}), q_i^{k(j)})) + \\ & \quad v^T (\nabla_w d(p(t_i^{k(j)}, w_{k(j)}), q_i^{k(j)}) - \nabla_w d(p(t, w_*), q)) + \\ & \quad v^T \nabla_w d(p(t, w_*), q) \\ &\geq -L_2 \beta^{k(j)} \epsilon - L_2 \|p(t_i^{k(j)}, w_{k(j)}) - p(t, w_*)\| \\ &\geq -L_2 \beta^{k(j)} \epsilon - L_2 \epsilon_4, \end{aligned}$$

For the first term above, we use our subdivision rule and continuity of  $\nabla_w d$ . For the second term, we use Lemma 6.6 by choosing  $j > j(\epsilon_4)$ . The third term is bigger than zero due to  $v$  violating the KKT condition. Next, we can invoke Lemma 6.4 and show that:

$$v^T \sum_{i \in S_{k(j)}} \lambda_i^{k(j)} \nabla g_i(w_{k(j)}) \leq L_3 L_4 \lambda (L_2 \beta^{k(j)} \epsilon + L_2 \epsilon_4).$$

Finally, our algorithm only consider differentiable objective function  $O$ , which is also Lipschitz continuous due to boundedness, with Lipschitz constant denoted as  $L_6$ . As a result, we have:

$$\begin{aligned} v^T O(w_{k(j)}) &= v^T (O(w_{k(j)}) - O(w_*)) + v^T O(w_*) \\ &\leq \epsilon_3 + L_6 \|w_{k(j)} - w_*\|. \end{aligned}$$

Combining all the results above, we conclude that:

$$\begin{aligned} & v^T \nabla_w [O(w_{k(j)} + \lambda B(w_{k(j)}, \mathcal{E}'))] \\ &\leq \epsilon_3 + L_6 \|w_{k(j)} - w_*\| + L_3 L_4 \lambda (L_2 \beta^{k(j)} \epsilon + L_2 \epsilon_4), \end{aligned}$$

which can be made arbitrarily close to  $\epsilon_3$  by choosing large enough  $j$ , contradicting the fact that  $w_{k(j)}$  is a local minimum of P-IPM. ■

We can now claim our main result:

**Corollary 6.7:** Any accumulation point of the sequence  $\{w_k\}$  satisfies the KKT condition of SIP (Equation 8) under Assumption 6.1 and Assumption 6.3.